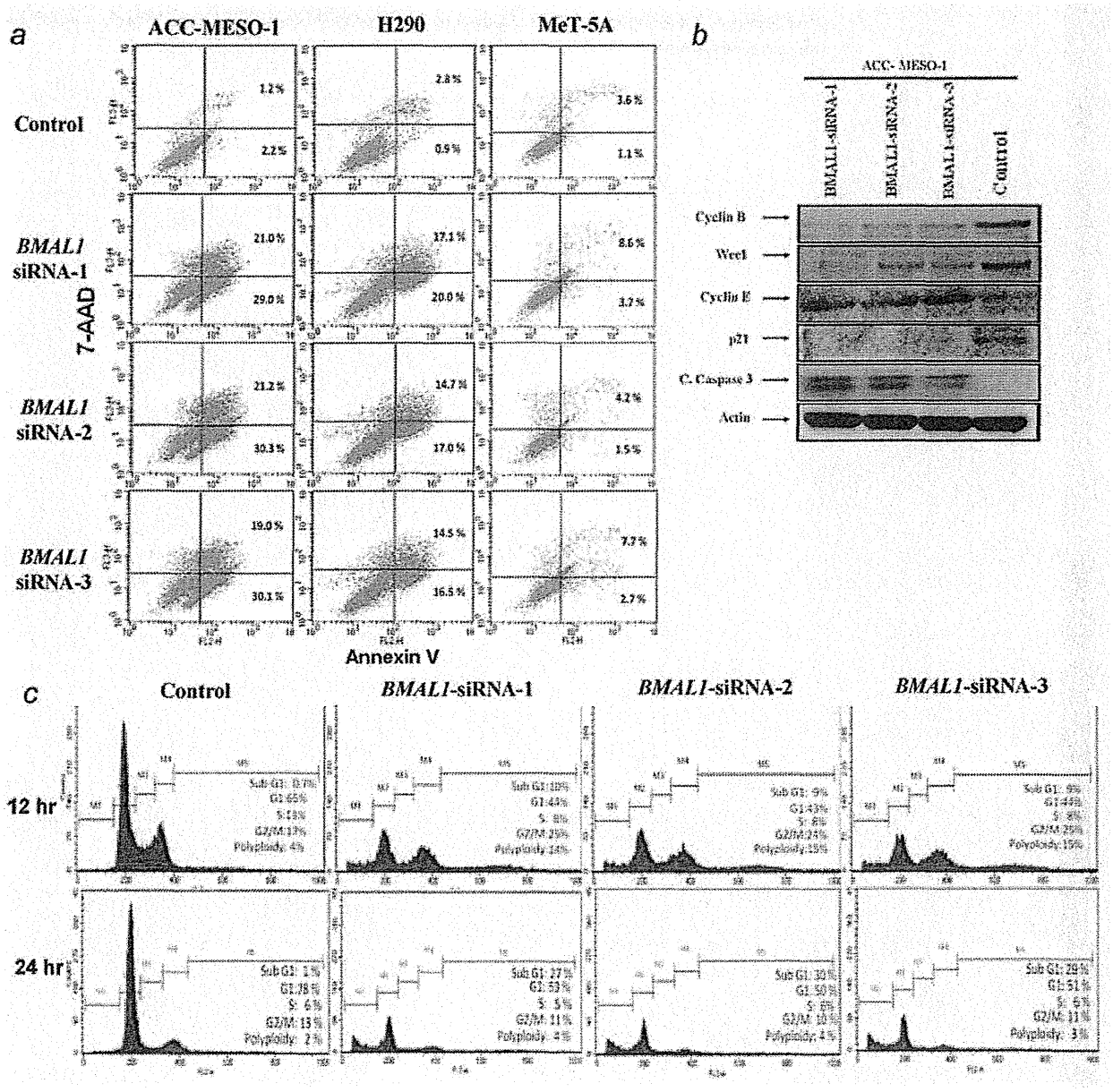

Figure 5.

BMAL1 knockdown induces apoptosis and cell cycle disruption (*a*) FACS analysis of cells costained with anti-annexin V and 7-AAD. High Annexin V and low 7-AAD cells are undergoing apoptosis while cells with low Annexin and high 7-AAD are undergoing necrosis. (*b*) Immunoblot showing effects of *BMAL1* knockdown on its targets in ACC-MESO-1 cells. (*c*) Cell cycle analysis of ACC-MESO-1 cells transfected with *BMAL1*-siRNA or control oligos. Forty-eight-hour post-transfection cells underwent serum starvation for 12 hr (upper panel) and for 24 hr (lower panel) then were harvested with both adherent and floating cells were combined and prepared for cell cycle analysis by flow cytometry, as described in "Material and Methods" Section. Results are the average of two

independent experiments. [Color figure can be viewed in the online issue, which is available at wileyonlinelibrary.com.]

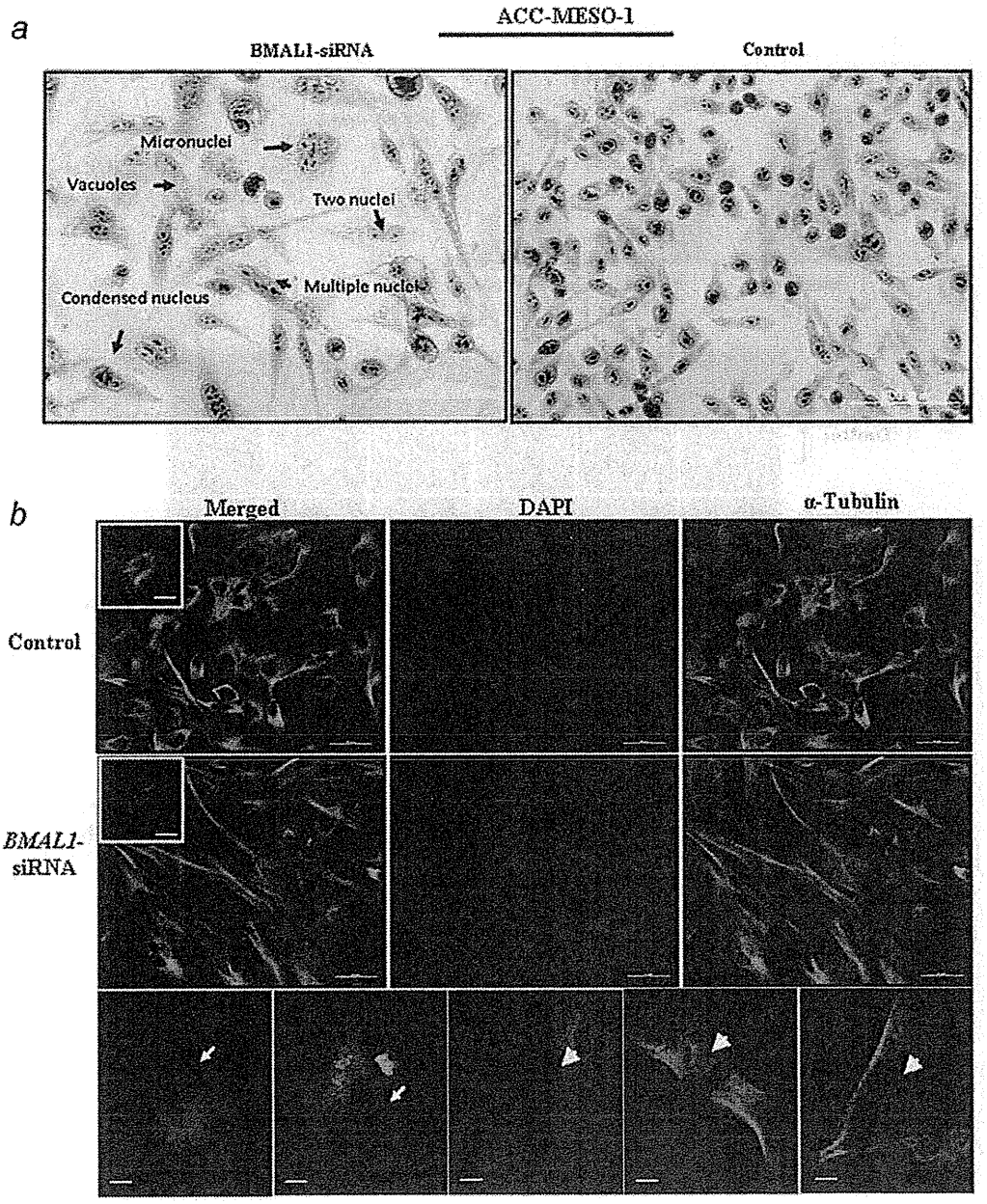

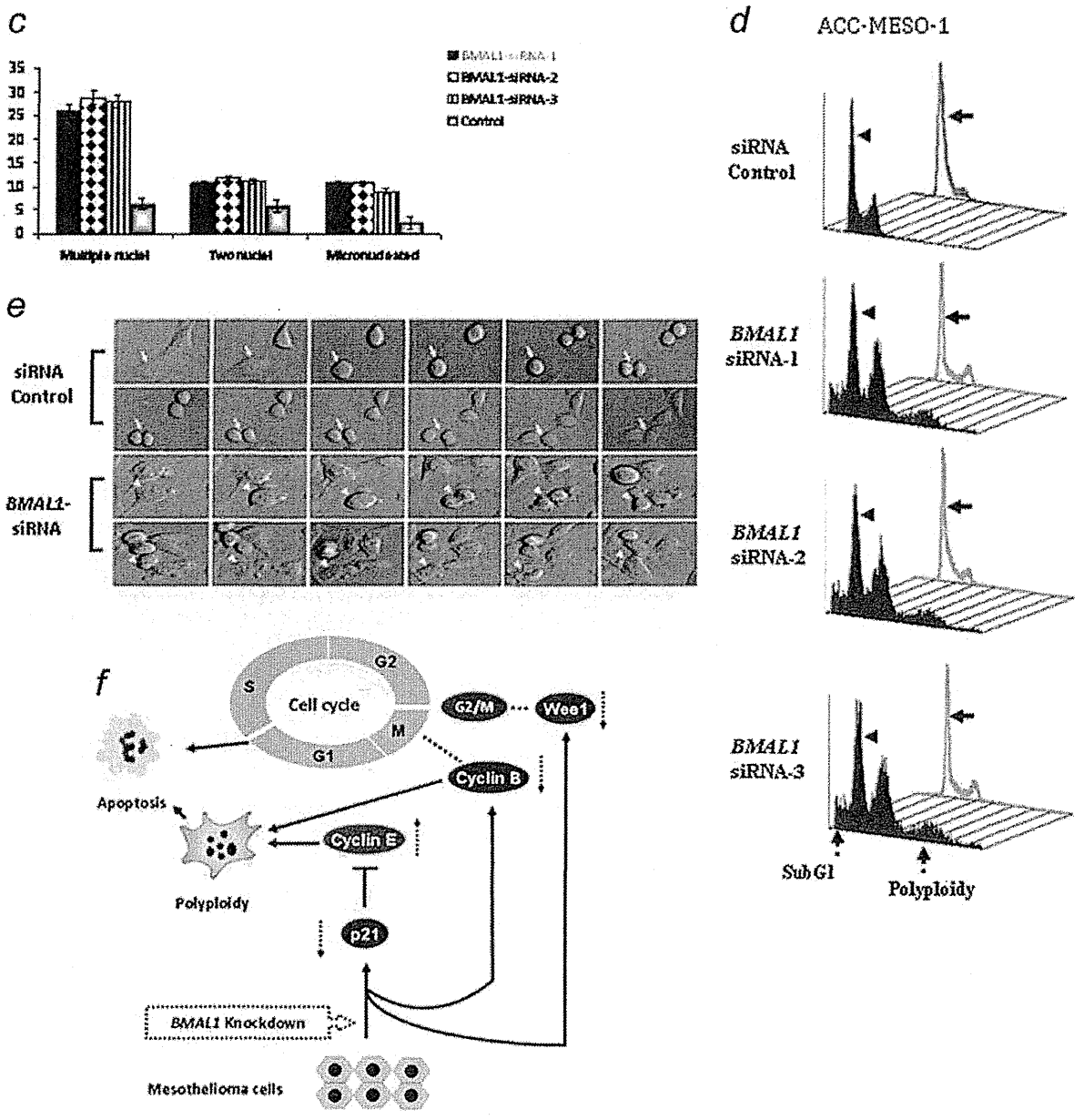

Figure 6.

BMAL1 knockdown induces dramatic morphological alterations in ACC-MESO-1 cells. (*a*) H–E stain showing the nuclear morphological changes identified in ACC-MESO-1 cells after ablation of *BMAL1*. (*b*) IF of α-tubulin and DAPI stains. The upper panels represent ACC-MESO-1 cells treated with siRNA control. The lower panels represent the most frequent morphological changes (arrow indicates micronucleation and arrow head indicates multiple nuclei) in single ACC-MESO-1 cell after *BMAL1* depletion. The middle panels represent ACC-MESO-1 cells treated with *BMAL1* siRNA. (*c*) Quantification of the binuclear, multinuclear and micronuclear phenotypes in ACC-MESO-1 cells after BMAL1 knockdown. (*d*) Cell cycle profiling of ACC-MESO-1 cells showing marked decrease of

BMAL1-induced cell death and polyploidy formation following mitosis block. ACC-MESO-1 cells transfected with *BMAL1* siRNA or control oligos with double-thymidine (black arrows) and without thymidine treatment (arrow heads) were harvested for analyses of DNA content by flow cytometry. Synchronized cells at late G1/early S by double-thymidine escaped from *BMAL1* knockdown-induced cell death with marked reduction in subG1 and polyploidy formation. (*e*) Time lapse microscopic examination showing the aberrant mitosis in ACC-MESO-1 cells transfected with *BMAL1* siRNA (white arrow head) and intact mitosis in cells transfected with control oligos (white arrow). (*f*) Proposed molecular mechanism of BMAL1 knockdown-induced mitotic catastrophe in ACC-MESO-1 cells. Decreasing cyclin B below a critical level results in mitosis skipping and enhances polyploidy formation. Downregulation of p21WAF1/CIP1 results in accumulation of cyclin E which could lead to increased number of polyploidy cells. Wee1 downregulation could contribute to eventual escape from G2/M arrest, which in turns participates in impairment of mitotic integrity. [Color figure can be viewed in the online issue, which is available at wileyonlinelibrary.com.]

Table 1

Clinical features of 16 patients with MPM

ID	Age/Sex	Histology	BMAL1 Status (IHC score)	Asbestos exposure	OS (M)	Staging		Surgery	Therapy
						Clinical	Pathological		
1	50/M	Biphasic	Negative (1+)	+	2.5	T2N0M0/II	T3N2M0/III	Right EPP	No
2	54/M	Biphasic	Negative (1+)	+	24.0	T2N0M0/II	T2N0M0/II	Left EPP	No
3	56/M	Epithelioid	Negative (1+)	+	25.3	T3N2M0/III	T4N0M0/IV	Left EPP	No
4	65/M	Epithelioid	Negative (0)	+	8.8	T3N1M0/III	T3N2M0/III	Right EPP	Neoadjuvant CT
5	46/F	Epithelioid	Negative (1+)	−	36.0	T1bN0M0/Ib	T3N2M0/III	Left EPP	Adjuvant CT + LRT
6	70/F	Epithelioid	Negative (0)	−	27.6	T1bN1M0/III	T2N1M0/III	Left EPP	Neoadjuvant CT
7	65/M	Epithelioid	Positive (3+)	+	8.4	T3N0M0/III	T4N0M0/IV	Right EPP	Neoadjuvant CT
8	60/M	Biphasic	Negative (0)	+	31.3	T3N2M0/III	T3N0M0/III	Right EPP	Neoadjuvant CT + PHR
9	62/M	Epithelioid	Positive (2+)	+	13.0	T3N0M0/III	T4NxM0/IV	Left pleurectomy	Neoadjuvant CT
10	67/M	Biphasic	Negative (1+)	−	11.6	T2N1M0/III	T3N0M0/III	Right EPP	Neoadjuvant CT + PHR
11	66/M	Biphasic	Negative (0)	+	8.3	T2N0M0/II	T3N0M0/III	Right EPP	Neoadjuvant CT
12	67/M	Epithelioid	Positive (2+)	+	3.6	T2N0M0/II	T3N2M0/III	Right EPP	No
13	68/M	Epithelioid	Positive (3+)	−	7.7	T3N0M0/III	T3N0M0/III	Left EPP	Neoadjuvant CT + PHR
14	63/M	Epithelioid	Positive (3+)	+	1.9	T2N0M0/II	T3N0M0/III	Lt EPP	Neoadjuvant CT
15	68/M	Sarcomatoid	Negative (0)	+	1.0	T3N2M0/III	T3N0M0/III	Right EPP	Neoadjuvant CT
16	64/M	Epithelioid	Negative (1+)	+	0.8	T2N0M0/II	T3N2M0/III	Left EPP	Neoadjuvant CT

Abbreviations: Id, patient's number; IHC, immunohistochemical score for *BMAL1*; OS, overall survival; M, month; EPP, extra-pleural pneumonectomy; neoadjuvant CT, neoadjuvant chemotherapy (cisplatin + pemetrexed); adjuvant chemotherapy (cisplatin + pemetrexed); LRT, local radiation therapy; PHR, post-operative hemithoracic radiation.

Tumor Biol. (2012) 33:2135–2141
DOI 10.1007/s13277-012-0473-5

RESEARCH ARTICLE

Effects of hyaluronic acid and CD44 interaction on the proliferation and invasiveness of malignant pleural mesothelioma

Takeshi Hanagiri · Shinji Shinohara · Masaru Takenaka · Yoshiki Shigematsu · Manabu Yasuda · Hidehiko Shimokawa · Yoshika Nagata · Makoto Nakagawa · Hidetaka Uramoto · Tomoko So · Fumihiro Tanaka

Received: 4 May 2012 / Accepted: 26 July 2012 / Published online: 11 August 2012

Abstract Hyaluronic acid (HA) has been proposed as a biochemical marker of malignant pleural mesothelioma (MPM). The present study focused on the implications of HA and CD44 interaction in the proliferation and invasiveness of MPM. The proliferation and invasive activity was evaluated in two human mesothelioma cell lines, ACC-MESO-1 and K921MSO, by the 3-(4,5-dimethylthiazol-2-yl)-2,5-diphenyltetrazolium bromide assay and the transwell chamber model. The knockdown of CD44 gene expression was accomplished by transfection of the cells with small interfering RNA. Flow cytometry revealed that both the ACC-MESO-1 and K921MSO cell lines highly expressed CD44. Treatment with HA enhanced the proliferation in both mesothelioma cell lines in comparison to cells without HA treatment. The treatment with HA (25 μg/ml) also significantly upregulated the invasion of both types of cells. The silencing of CD44 significantly abrogated the effect of HA treatment on the proliferation of ACC-MESO-1 cells and significantly suppressed the proliferation of K921MSO cells. HA–CD44 binding is important for the migration and proliferation of mesothelioma cells. Therefore, the HA–CD44 interaction is a potentially useful therapeutic target in MPM.

Keywords Malignant pleural mesothelioma · Hyaluronic acid · CD44 · Proliferation

T. Hanagiri (✉) · S. Shinohara · M. Takenaka · Y. Shigematsu · M. Yasuda · H. Shimokawa · Y. Nagata · M. Nakagawa · H. Uramoto · T. So · F. Tanaka
Second Department of Surgery, School of Medicine, University of Occupational and Environmental Health, Yahatanishi, Kitakyushu 807, Japan
e-mail: hanagiri@med.uoeh-u.ac.jp

Introduction

Malignant pleural mesothelioma (MPM) is an aggressive neoplasm arising from mesothelial cells, and it has an extremely poor prognosis. MPM is closely related to previous exposure to asbestos fibers. Due to the widespread use of asbestos fibers in the latter half of the twentieth century, the incidence of MPM is predicted to increase sharply in industrialized countries within the next few decades after a 30- to 40-year latency period [1, 2]. In Japan, about 500 patients with mesothelioma died in 1995, and the number of deaths increased to approximately 900 patients in 2003 and to 1,170 in 2008 [3]. Murayama et al. reported that there would be about 100,000 deaths in Japan due to MPM during the next 40 years [4]. Not only occupational exposure but also environmental exposure, present a public health problem, because asbestos was used widely in buildings as a construction material and asbestos cement pipes [5, 6].

MPM is difficult to diagnose at an early stage and often progresses to an advanced stage without symptoms. Although a new chemotherapy regimen using *cis*-diamminedichloroplatinum plus pemetrexed has led to some improvement in the prognosis, the median survival is generally only 9–12 months [7–9]. The best potentially curative approach to MPM seems to be extrapleural pneumonectomy (EPP) at an early stage, followed by chemotherapy and radiotherapy (trimodal treatment). Sugarbaker et al. reported that the median survival after EPP was 19 months, and that the 2- and 5-year survival rates were 38 and 15 %, respectively [9]. However, the perioperative mortality of EPP has been reported to be as high as 11 % [9]. In addition to the conventional therapies such as surgery, chemotherapy, and radiotherapy, the development of alternative therapies, such as molecular targeted therapy or gene therapy is highly desired.

Pleural effusion is the initial clinical sign in more than 90 % of patients with MPM. High concentrations of hyaluronic acid (HA) in pleural fluid from patients with malignant mesothelioma have been demonstrated in a number of studies, and this finding is an important auxiliary finding for the diagnosis of this tumor [10]. HA is a linear glycosaminoglycan, which is ubiquitously distributed in the extracellular matrix and interacts with cell surface receptors including CD44 [11]. Hyaluronan plays an essential physiological role in processes such as cell growth, differentiation, adhesion, and cell migration [12]. CD44 is a polymorphic transmembrane glycoprotein that modulates a wide variety of cell–cell and cell–matrix interactions, including those related to cell adhesion, motility, and matrix degradation [13]. The present study focused on the implications of HA and the CD44 receptor in the proliferation and invasiveness of MPM.

Materials and methods

The institutional review board approved this study, and informed consent was obtained from the patient for the use of their specimens to establish a mesothelioma cell line "K921MSO," and to perform analyses on this cell line. The HA used in the present experiments was ultra-low molecular weight HA purchased from R&D systems (Minneapolis, MN). Molecular weight was 7.46 kDa (range, 2–8 kDa). HA was dissolved in distilled water-based phosphate-buffered saline (PBS).

Cell lines

The human mesothelioma cell lines, ACC-MESO-1 and K921MSO, were established at the Aichi Cancer Center Research Institute (Nagoya, Japan) [14] and in our laboratory [15], respectively. The original tumors of ACC-MESO-1 mainly consisted of epithelioid cells, and K921MSO was established from a sarcomatoid type tumor. The original tumors of ACC-MESO-1 and ACC-MESO-4 mainly consisted of epithelioid cells, The cells were maintained in culture medium at 37 °C in a 5 % CO_2 atmosphere. The culture medium contained RPMI 1640 (Gibco BRL, Grand Island, NY) supplemented with 10 % heat-inactivated fetal calf serum (FCS) (Equitech-bio, Ingram, TX), 10 mM HEPES, 100 IU/mL penicillin G, and 100 mg/mL streptomycin sulfate [15]. A sandwich-binding assay using HA-binding protein was used for measuring the serum HA level in the culture medium (Chugai/Reads Medical Products, Westminster, CO).

Flow cytometry

After the tumor cell lines were harvested by trypsinization, they were washed twice and resuspended in PBS with 1 % human AB serum. A fluorescein isothiocyanate (FITC)-conjugated mouse anti-human CD44 monoclonal antibody (mouse IgG2b) was purchased from BD Biosciences (Bedford, MA). The cells were incubated for 30 min at 37 °C with an anti-CD44 antibody (20 nM each) coupled with FITC in the dark. Afterwards, the cells were washed twice again, fixed with 0.5 % formaldehyde, and then were analyzed on a FACS Calibur flow cytometer (BD Biosciences) using the FlowJo software package (Tree Star Inc., OR).

Proliferation assay

The 3-(4,5-dimethylthiazol-2-yl)-2,5-diphenyltetrazolium bromide (MTT) Cell Proliferation Assay (ATCC, Manassas, VA) was performed as described below. Tumor cells were seeded at 1,000 cells per well into 96-well plates in triplicate with and without HA (25 μg/ml). The control wells (HA−) were exposed to diluent (PBS) only. The tumor cells were incubated for 48 h with and without HA treatment, and then 10 μL of the MTT Reagent was added to each well. After incubation for 2 to 4 h, 100 μL of the detergent reagent was added, and the cells were left at room temperature in the dark for 2 h. The absorbance was read at 570 nm using a reference wavelength of 690 nm. The amount of color produced was directly proportional to the number of viable cells. The proliferation index was calculated using the following formula:

Proliferation index = absorbance at 540 nm 48 h after incubation /absorbance at 540 nm before incubation.

The results are expressed as the mean values ± standard deviation (SD) of triplicate wells for each condition.

Concentration of soluble CD44 in the culture supernatant

The concentration of soluble CD44 in the culture supernatant was measured according to the manufacturer's instructions using a commercially available sandwich enzyme-linked immunosorbent assay kit (ELISA; eBiosource, San Diego, CA). The sensitivity of kit was 0.02 ng/ml for CD44. Assays were performed according to the manufacturer's instructions. Briefly, a specific monoclonal antibody was coated in the wells of 96-well microtiter plates. The CD44 present in the culture supernatant or in the standard bound to antibodies adsorbed to each wells. A horseradish peroxidase-conjugated monoclonal antibody against CD44

was added. After incubation, the unbound enzyme-conjugated antibodies were removed by washing and a substrate solution was added to each well. The optical density of each sample well was measured at 450 nm. A standard curve was prepared from six standard dilutions of antigens. The coloring reaction was terminated by the addition of stop solution, and the absorbance was measured at 450 nm on an ELISA plate reader. The results are expressed as the mean values±SD of triplicate wells for each condition.

Invasion assay

The cell invasion assay was performed with the BD BioCoat™ Matrigel™ Invasion Chamber (BD Biosciences). In the invasion chambers, filters with an 8-μm pore size were coated with BD Matrigel™ and reconstituted at 37 °C with DMEM before use. After rehydration, the medium was carefully removed. Tumor cell suspensions (5×104 cells/filter) were added to the upper compartment (of a 24-well plate), whereas the bottom wells were immediately filled with or without 25 μg/ml of HA as a chemo-attractant. The control wells (HA−) were exposed to the diluent (PBS) alone. After a 48-h incubation with and without HA treatment, the nonmigrated and noninvasive cells in the upper chamber were carefully removed, and the adherent cells present on the lower surface of the insert were fixed with methanol and stained with Giemsa dye. The cells that had migrated and invaded were quantified by light microscopy. The cells were always counted microscopically in five randomly chosen fields (magnification, ×200) of the triplicate membranes. The data are expressed as the number of cells that invaded through the Matrigel matrix. The percentage of invasive cells was calculated as the percent invasion through the matrigel membrane treated with HA relative to the migration through the membrane without HA (control wells). The results are expressed as the mean values ± SD.

Suppression of CD44 expression by RNA interference

Three stealth RNA interference (RNAi) sequences against CD44 were synthesized by Invitrogen. The siRNA sequences used were as follows: siRNA1-GCAAGUCUCAGGAAAU GGUGCAUUU and AAAUGCACCAUUUCCUGAGA CUUGC; siRNA2- GCUGACCUCUGCAAGGCUUU CAAUA and UAUUGAAAGCCUUGCAGAGGUCAGC; and siRNA3-GAACAAGGAGUCGUCAGAAACUCCA and UGGAGUUUCUGACGACUCCUUGUUC. The siRNA was transfected into the mesothelioma cell lines using Lipofectamine 2000 (Invitrogen). A control siRNA sequence, commercially available stealth RNAi negative control medium GC duplex (Invitrogen), was also used in each experiment. RNA interference was performed according to the manufacturer's instructions as follows; 20 μM Stealth™ RNAi were diluted in 200 μl Opti-MEM® and mixed gently. Lipofectamine™ 2000 (5 μl) was diluted in 200 μl Opti-MEM®, then mixed gently and incubated for 5 min at room temperature. After the 5-min incubation, the diluted Stealth™ RNAi was combined with the diluted Lipofectamine™ 2000, and mixed gently and incubated for 20 min at room temperature.

The Stealth™ RNAi -Lipofectamine™ 2000 complexes were added to each well containing cells and mixed gently. Then, the transfected cells were diluted with RPMI 1640 containing 1 % FCS, and 1×10^4 cells were seeded onto the upper chamber of Matrigel Invasion Chamber plates in triplicate. The lower chamber of the transwell was filled with 750 μl of culture media with or without 25 μg/ml HA as an adhesive substrate. The effects of the RNAi were evaluated by flow cytometry with a CD44 antibody. Each stealth siRNA sequence efficiently suppressed the surface expression of the CD44 molecule 24–72 h after transfection, but siRNA1 was the most effective. Therefore, we decided to use siRNA1 for all further experiments. After the silencing of CD44 by siRNA, the proliferation and invasion activity of the mesothelioma cell lines were evaluated during the 48-h incubation with or without HA as described above.

Statistical analyses

The comparisons between two groups were performed using Student's *t* test or the Mann–Whitney *U* test. The differences were considered to be significant for $p<0.05$. The Statview

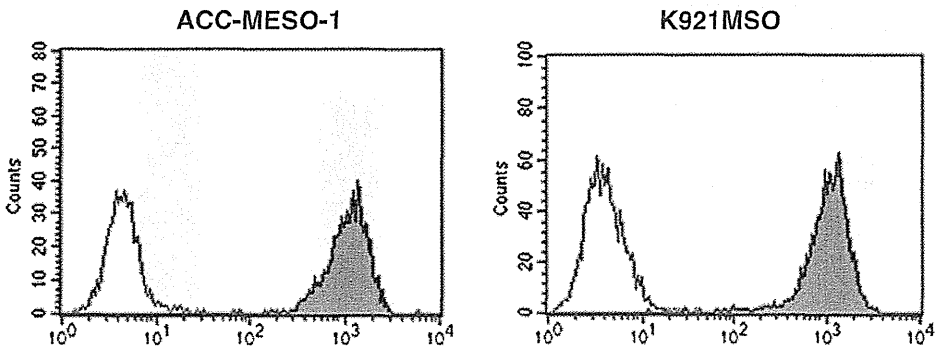

Fig. 1 The CD44 expression of the mesothelioma cell lines. The expression of CD44 was evaluated by flow cytometry with a FITC-conjugated monoclonal antibody. Isotype control antibody (*open histogram*); CD44 antibody (*filled histogram*)

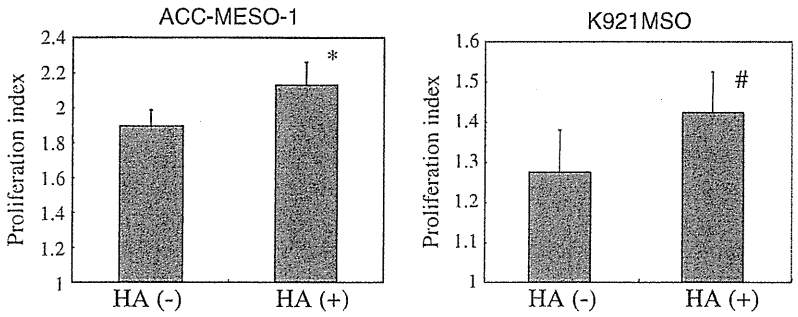

Fig. 2 Effect of hyaluronic acid (*HA*) on proliferation of mesothelioma cell lines. The tumor cells were incubated for 48 h with or without HA treatment, and the proliferation of the mesothelioma cell lines was evaluated by the MTT cell proliferation assay. The control wells (*HA*−) were exposed to diluent (PBS) alone. The proliferation of mesothelioma cell lines was enhanced by hyaluronic acid (*HA*) treatment (25 μg/ml). The data are presented as the mean values±SD of triplicate wells for each condition. *p=0.048; #p=0.107

V software package (Abacus Concept, Berkeley, CA) was used for all of the statistical analyses.

Results

Flow cytometry revealed that both the ACC-MESO-1 and K921MSO cell lines highly expressed the CD44 (Fig. 1). The cell proliferation was evaluated by the MTT cell proliferation assay 48 h after the addition of 25 μg/ml HA. Treatment with HA significantly enhanced the proliferation of ACC-MESO-1 cells in comparison with the untreated cells (p=0.045). The K921MSO cells also tended to show increased proliferation after HA treatment (p=0.107) (Fig. 2). In this experiment, the concentration of soluble CD44 in the culture supernatant was measured 48 h after incubation with or without 25 μg/ml HA by using ELISA. The level of soluble CD44 in the both supernatant of ACC-MESO-1 and K921MSO was significantly increased by addition of HA, compared with that incubated without HA (Fig. 3). The soluble CD44 was not detected in the culture medium before incubation of these two cell lines. The invasion activity was evaluated using a Matrigel™ Invasion Chamber 48 h after the addition of 25 μg/ml HA. The percentage of invasive cells treated with HA increased up to 172±17 and 188±47 % in the ACC-MESO-1 and K921MSO cell lines, respectively. The treatment with HA (25 μg/ml) significantly upregulated the invasion of both the ACC-MESO-1 and K921MSO cell lines.

To assess the secretion of HA, the concentration of HA in the cell culture medium was measured 48 h after incubation. The concentration of HA was 50 ng/ml before incubation and increased to 78 ng/ml in the ACC-MESO-1 culture and to 83 ng/ml in the K921MSO culture during the 48-h incubation.

siRNA-mediated silencing of CD44 was performed in ACC-MESO-1 and K921MSO cells in order to determine the impact of the protein on the cell proliferation and invasion. The efficiency of the knockdown was confirmed by flow cytometry 72 after transfection of the CD44-specific and control siRNA (Fig. 4). The suppression of CD44 expression was efficient, with the CD44 transcripts being reduced to 10 % of the control levels. After suppression by siRNA, the proliferation activity of the mesothelioma cell lines were evaluated during the 48 h incubation with or without HA as described above. The silencing of CD44 significantly abrogated the effect of HA treatment on the proliferation of ACC-MESO-1 cells (Fig. 5). The

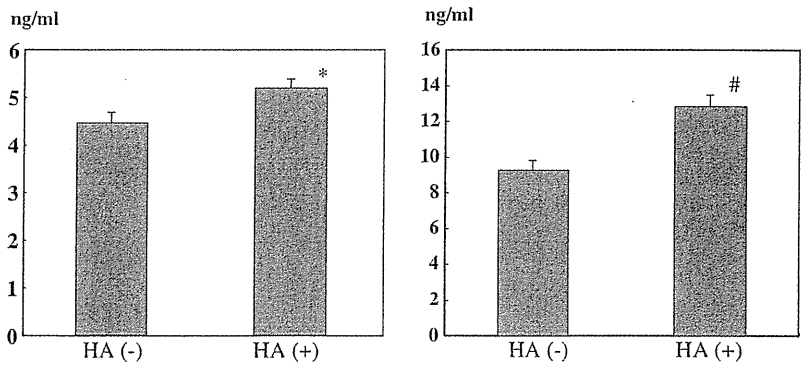

Fig. 3 The level of soluble CD44 in the both supernatant of mesothelioma cell lines. The concentration of soluble CD44 in the culture supernatant was measured 48 h after incubation with or without 25 μg/ml HA by using an ELISA. The data are presented as the mean values±SD of triplicate wells for each condition. *p=0.009; #p=0.001

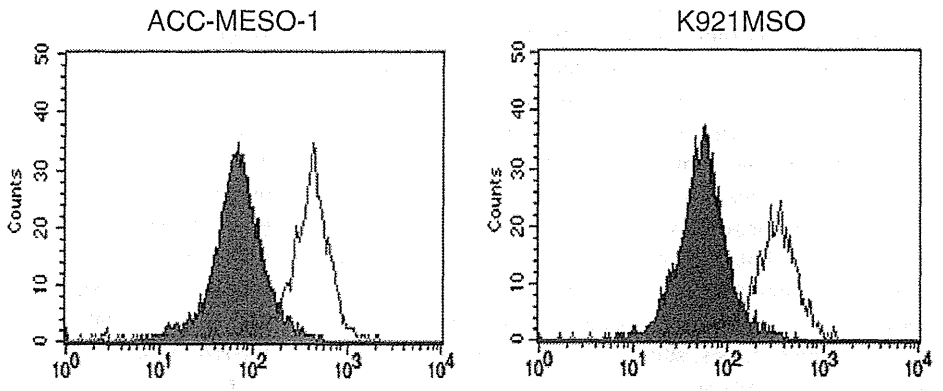

Fig. 4 The downregulation of CD44 expression on mesothelioma cell lines following siRNA-mediated silencing. Flow cytometry revealed that the expression of CD44 was suppressed 72 h after transfection with the CD44-siRNA. Control siRNA (*open histogram*); CD44-targeted siRNA (*filled histogram*)

proliferation of the K921MSO cells was also significantly suppressed by the silencing of CD44, but an increase in the effect of HA treatment was observed (Fig. 5). The percentage of invasive ACC-MESO-1 cells after the silencing of CD44 decreased significantly to 59±8 % as compared with those transfected with a control siRNA (p=0.009).

Discussion

Most of patients with MPM are suffering from a pleural effusion at the time of presentation, and this is a major clinical sign that often initiates the diagnostic process [16]. Elevated levels of HA in effusions are sensitive diagnostic indicators of MPM. There is a controversy regarding a suitable cut-off value of HA in the pleural effusion. Welker et al. reported that the highest diagnostic reliability of a MPM diagnosis was found at 30 mg/l of HA values in pleural fluids [17]. Thylén et al. reported that an elevated level of HA was an unfavorable prognostic factor [10]. The present study focused on the effects of HA on the proliferation and invasiveness of MPM through the CD44 receptor.

HA is a glycosaminoglycan composed of 2,000–25,000 disaccharides of glucuronic acid and *N*-acetylglucosamine, giving rise to molecules with weights ranging from 105–107 Daltons [18]. Although HA is distributed ubiquitously in connective, epithelial, and neural tissues as a major extracellular matrix component, its organization and function with respect to cells and tissues are variable. HA is known to facilitate cell adhesion, motility, proliferation and tumor progression. MPM is characterized by the accumulation of abundant intracellular HA, and elevated levels of HA in pleural fluid are indicative of MPM [10]. Hyaluronan is produced on the surface of the plasma membrane by specific hyaluronan synthases (HAS) [19]. Dysregulation of HAS genes results in the abnormal production of HA and promotion of abnormal biological processes, such as transformation and metastasis [20]. Low molecular weight hyaluronan

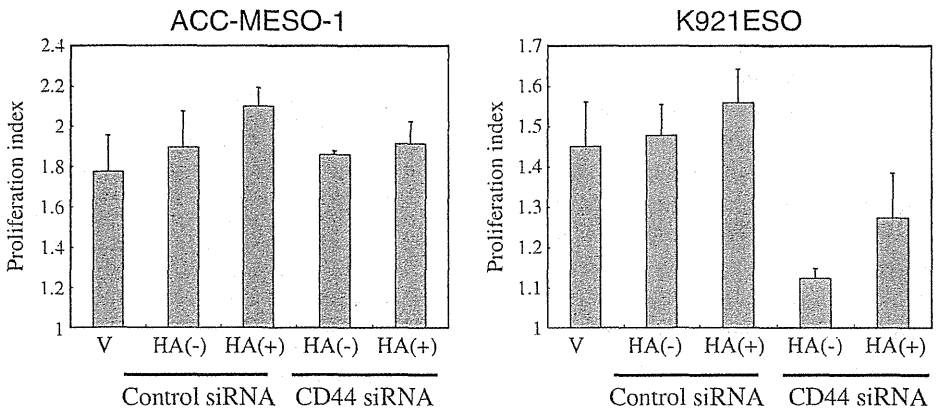

Fig. 5 The effects of siRNA-mediated silencing of CD44 on the proliferation of mesothelioma cell lines. The silencing of CD44 significantly decreased the effect of HA treatment on the proliferation of ACC-MESO-1 cells. The proliferation of the K921MSO cells was also significantly suppressed by the silencing of CD44, but the increase in proliferation following HA treatment remained. The wells without HA were treated with a corresponding amount of PBS (the diluent alone). *V* vehicle only (Lipofectamine only). The data are presented as the mean values ± SD of triplicate wells for each condition

is thought to contribute to the pericellular matrix, or may interact with cell surface HA receptors, triggering signaling cascades that leads to profound changes in cell behavior.

CD44, the principal receptor for hyaluronan, is one of the adhesion molecules which is essential for cell–cell and cell–matrix interactions. The HA–CD44 interactions stimulate a variety of downstream processes associated with tumor progression or cellular transformation [21, 22]. These interactions are important for a variety of aspects of tumor pathobiology, including anchorage-independent growth, migration, angiogenesis, suppression of apoptosis, and metastasis. In the present study, we demonstrated that the treatment of HA increased their proliferation and invasion of CD44-positive mesothelioma cell lines. The HA–CD44 interaction leads to CD44-epidermal growth factor receptor (EGFR) complex formation [23]. HA treatment was shown to promote the phosphorylation of the EGFR, activating the EGFR tyrosine kinase and promoting the activation of downstream EGFR-mediated signaling pathways, including the Ras, RhoA, Rho kinase, and phosphatidylinositol-3 kinase pathways [23].

The soluble CD44 in the supernatant of cell culture medium increased after HA treatment in both the ACC-MESO-1 and K921MSO cell lines. Stamenkovic et al. previously reported that CD44-dependent migration requires CD44 to be shed from the cell surface, and matrix metalloproteinase-mediated cleavage may be involved in the underlying mechanism [24]. The proteolytic cleavage of CD44 results in the formation of a soluble extracellular part of CD44 that most likely regulates cell migration, and then the CD44 intracellular domain translocates to the nucleus and promotes the transcription of several genes, including that encoding CD44 itself, which provides a positive feedback regulatory mechanism for CD44 expression [25]. Goebeler et al. reported that the shedding of CD44 from the cell surface after the binding of HA promoted melanoma cell motility, and that the mechanism was associated with an autocrine secretion of HA [26]. The HA concentration in the supernatant of the culture medium was increased after 48 h of incubation in both cell lines (ACC-MESO-1 and K921MSO) examined in the present study. Mesothelioma cells appear to generate HA that binds to their own CD44. Furthermore, HA is deposited within the pulmonary microvessels, where it may serve as a ligand for CD44. The CD44–HA interaction has been shown to play a major role in leukocyte endothelial cell adhesion and extravasation [27]. This mechanism is also relevant for tumor cell adhesion and extravasation, which results in pulmonary metastases [28].

The silencing of CD44 by siRNA abrogated the effect of HA treatment on the proliferation of ACC-MESO-1 cells, and it led to a significant inhibition of the proliferation of K921MSO cells. The silencing of CD44 also demonstrated a suppressive effect on the invasion of ACC-MESO-1 cells. In a previous study, the downregulation of CD44 expression by siRNA in an ovarian cancer cell line inhibited the tumor growth, invasion and resistance to apoptosis [29]. Sugahara et al. also reported that the effect of HA treatment on cell migration was inhibited by an anti-CD44 mAb (BRIC235), which blocked the HA–CD44 interaction [30]. The HA–CD44 interaction can activate the Ras/mitogen-activated protein kinase (MAPK) signaling pathway [31]. Pretreatment of cells with MAPK inhibitors may further suppress the HA-induced tumor growth.

The present study has shown that HA and CD44 interaction is important for mesothelioma cells, and that they are involved in regulating their migration and proliferation. Therefore, the HA–CD44 interaction is a potentially important therapeutic target in MPM, and a better understanding of the signaling mechanisms involving CD44 may be useful for the development of a novel HA-based anticancer therapy.

Acknowledgments This study was supported in part by a UOEH Research Grant for the Promotion of Occupational Health and a Grant-in-Aid for scientific research from the Ministry of Education, Culture, Sports, Science and Technology, Japan. We thank Yukari Furutani, Misako Fukumoto, and Yukiko Koyanagi for their expert technical help.

Conflicts of interest None

References

1. Peto J, Hodgson JT, Matthews FE, et al. Continuing increase in mesothelioma mortality in Britain. Lancet. 1995;345:535–9.
2. Peto J, Decarli A, La Vecchia C, Levi F, Negri E. The European mesothelioma epidemic. Br J Cancer. 1999;79:666–72.
3. Gemba K, Fujimoto N, Kato K, Aoe K, Takeshima Y, Inai K, et al. National survey of malignant mesothelioma and asbestos exposure in Japan. Cancer Sci. 2012;103:483–90.
4. Murayama T, Takahashi K, Natori Y, Kurumatani N. Estimation of future mortality from pleural malignant mesothelioma in Japan based on an age-cohort model. Am J Ind Med. 2006;49:1–7.
5. Marinaccio A, Scarselli A, Binazzi A, et al. Asbestos related diseases in Italy: an integrated approach to identify unexpected professional or environmental exposure risks at municipal level. Int Arch Occup Environ Health. 2008;81:993–1001.
6. Maule MM, Magnani C, Dalmasso P, Mirabelli D, Merletti F, Biggeri A. Modeling mesothelioma risk associated with environmental asbestos exposure. Environ Health Perspect. 2007;115:1066–71.
7. Vogelzang NJ, Rusthoven JJ, Symanowski J, Denham C, Kaukel E, Ruffie P, et al. Phase III study of pemetrexed in combination with cisplatin versus cisplatin alone in patients with malignant pleural mesothelioma. J Clin Oncol. 2003;21:2636–44.
8. Jänne PA, Wozniak AJ, Belani CP, Keohan ML, Ross HJ, Polikoff JA, et al. Pemetrexed expanded access program investigators. Pemetrexed alone or in combination with cisplatin in previously treated malignant pleural mesothelioma: outcomes from a phase IIIB expanded access program. J Thorac Oncol. 2006;1:506–12.

9. Sugarbaker DJ, Flores RM, Jaklitsch MT, Richards WG, Strauss GM, Corson JM, et al. Resection margins, extrapleural nodal status, and cell type determine postoperative long-term survival in trimodality therapy of malignant pleural mesothelioma: results in 183 patients. J Thorac Cardiovasc Surg. 1999;117:54–63.
10. Thylén A, Hjerpe A, Martensson G. Hyaluronan content in pleural fluid as a prognostic factor in patients with malignant pleural mesothelioma. Cancer. 2001;92:1224–30.
11. Hillerdal G, Lindqvist U, Engström-Laurent A. Hyaluronan in pleural effusions and in serum. Cancer. 1991;67:2410–4.
12. Laurent TC, Laurent UB, Fraser JR. Functions of hyaluronan. Ann Rheum Dis. 1995;54:429–32.
13. Marhaba R, Zöller M. CD44 in cancer progression: adhesion, migration and growth regulation. J Mol Histol. 2004;35:211–31.
14. Usami N, Fukui T, Kondo M, Taniguchi T, Yokoyama T, Mori S, et al. Establishment and characterization of four malignant pleural mesothelioma cell lines from Japanese patients. Cancer Sci. 2006;97:387–94.
15. Shigematsu Y, Hanagiri T, Kuroda K, Baba T, Mizukami M, Ichiki Y, et al. Malignant mesothelioma-associated antigens recognized by tumor-infiltrating B cells and the clinical significance of the antibody titers. Cancer Sci. 2009;100:1326–34.
16. Baas P, Schouwink H, Zoetmulder FA. Malignant pleural mesothelioma. Ann Oncol. 1998;9:139–49.
17. Welker L, Müller M, Holz O, Vollmer E, Magnussen H, Jörres RA. Cytological diagnosis of malignant mesothelioma—improvement by additional analysis of hyaluronic acid in pleural effusions. Virchows Arch. 2007;450:455–61.
18. Laurent TC, Laurent UB, Fraser JR. The structure and function of hyaluronan: an overview. Immunol Cell Biol. 1996;74:A1–7.
19. Itano N, Sawai T, Atsumi F, Miyaishi O, Taniguchi S, Kannagi R, et al. Selective expression and functional characteristics of three mammalian hyaluronan synthases in oncogenic malignant transformation. J Biol Chem. 2004;279:18679–87.
20. Li Y, Li L, Brown TJ, Heldin P. Silencing of hyaluronan synthase 2 suppresses the malignant phenotype of invasive breast cancer cells. Int J Cancer. 2007;120:2557–67.
21. Twarock S, Tammi MI, Savani RC, Fischer JW. Hyaluronan stabilizes focal adhesions, filopodia, and the proliferative phenotype in esophageal squamous carcinoma cells. J Biol Chem. 2010;285:23276–84.
22. Wang SJ, Bourguignon LY. Role of hyaluronan-mediated CD44 signaling in head and neck squamous cell carcinoma progression and chemoresistance. Am J Pathol. 2011;178:956–63.
23. Bourguignon LY, Gilad E, Brightman A, Diedrich F, Singleton P. Hyaluronan–CD44 interaction with leukemia-associated RhoGEF and epidermal growth factor receptor promotes Rho/Ras co-activation, phospholipase Cε–Ca^{2+} signaling, and cytoskeleton modification in head and neck squamous cell carcinoma cells. J Biol Chem. 2006;281:14026–40.
24. Stamenkovic I, Yu Q. Shedding light on proteolytic cleavage of CD44: the responsible sheddase and functional significance of shedding. J Invest Dermatol. 2009;129:1321–4.
25. Nagano O, Saya H. Mechanism and biological significance of CD44 cleavage. Cancer Sci. 2004;95(12):930–5.
26. Goebeler M, Kaufmann D, Bröcker EB, Klein CE. Migration of highly aggressive melanoma cells on hyaluronic acid is associated with functional changes, increased turnover and shedding of CD44 receptors. J Cell Sci. 1996;109:1957–64.
27. Nandi A, Estess P, Siegelman MH. Hyaluronan anchoring and regulation on the surface of vascular endothelial cells is mediated through the functionally active form of CD44. J Biol Chem. 2000;275:14939–48.
28. Richter U, Wicklein D, Geleff S, Schumacher U. The interaction between CD44 on tumour cells and hyaluronan under physiologic flow conditions: implications for metastasis formation. Histochem Cell Biol. 2012;137:687–95.
29. Li CZ, Liu B, Wen ZQ, Li HY. Inhibition of CD44 expression by small interfering RNA to suppress the growth and metastasis of ovarian cancer cells in vitro and in vivo. Folia Biol. 2008;54:180–6.
30. Sugahara KN, Hirata T, Hayasaka H, Stern R, Murai T, Miyasaka M. Tumor cells enhance their own CD44 cleavage and motility by generating hyaluronan fragments. J Biol Chem. 2006;281:5861–8.
31. Sohara Y, Ishiguro N, Machida K, Kurata H, Thant AA, Senga T, et al. Hyaluronan activates cell motility of v-Src-Transformed cells via Ras-mitogen-activated protein kinase and phosphoinositide3-kinase-Akt in a tumor-specific manner. Mol Biol Cell. 2001;12:1859–68.

Laparoscopic Thoracic Duct Clipping for Persistent Chylothorax After Extrapleural Pneumonectomy

Norifumi Tsubokawa, MD, Yoichi Hamai, MD, Jun Hihara, MD, Manabu Emi, MD, Yoshihiro Miyata, MD, and Morihito Okada, MD

Department of Surgical Oncology, Research Institute for Radiation Biology and Medicine, Hiroshima University, Hiroshima, Japan

We describe a 68-year-old man who was treated by laparoscopic thoracic duct clipping for persistent chylothorax after an extrapleural pneumonectomy for malignant pleural mesothelioma. Initial conservative treatment did not resolve the postoperative chylothorax. A second surgery through the thoracic approach was considered invasive and difficult after extrapleural pneumonectomy. A laparoscopic approach proved effective and resolved the chylothorax. Thus, laparoscopic thoracic duct clipping is considered very useful for treating chylothorax.

(Ann Thorac Surg 2012;93:e131–2)

The reported incidence rate of postoperative chylothorax after extrapleural pneumonectomy (EPP) is 6% to 8% [1, 2]. Worsening of this complication occasionally leads to cardiopulmonary dysfunction, immunosuppression, electrolyte derangement, hypoproteinemia, and ultimately, sepsis and death [3]. Here, we describe postoperative chylothorax that was successfully managed by laparoscopic surgery after EPP.

Chest radiography revealed pleural fluid and pleural thickening in the left lung of a 68-year-old man with a history of exposure to asbestos. He had undergone open biopsy of the pleura at another hospital and the pathologic diagnosis based on the biopsy specimens was epithelial malignant pleural mesothelioma (MPM). He was referred to our hospital for further treatment. Thoracic computed tomography also revealed pleural effusion and overall pleural thickening, as well as partial tumor involvement of the outer aspect of the pericardium and diaphragm without penetration. We considered that the tumor was probably resectable because it had not extended into the soft tissues and ribs in the chest wall and mediastinal lymph nodes were not enlarged. Trimodal therapy, comprising induction chemotherapy with pemetrexed plus cisplatin, EPP, and postoperative radiation therapy, is reportedly feasible with reasonable long-term survival rates for patients with clinical stage I to III MPM [4]. We similarly performed 3 cycles of induction chemotherapy with 75 mg/m^2 of cisplatin on day 1 and 500 mg/m^2 of pemetrexed on day 1 at an interval of 3 weeks. Computed tomography showed that the tumor had decreased. Left EPP then proceeded with resection of the chest wall, including previous biopsy sites and a portion of the diaphragm and pericardium through a left thoracotomy, and complete resection was achieved. The previous open pleural biopsy had proceeded through several large intercostal thoracotomies. Therefore, we resected portions of 6 ribs that were located sufficiently far from these biopsy sites to eliminate the potential for tumor seeding. We extensively reconstructed the chest wall and diaphragm using DUALMESH (W.L. Gore & Associates Inc, Flagstaff, AZ) and the pericardium using a Gore-Tex sheet (W.L. Gore & Associates Inc).

We diagnosed postoperative chylothorax based on daily lactescent drainage of over 1,500 mL after oral intake that became evident on postoperative day (POD) 4. Conservative therapy comprised a low-fat diet with medium chain triglycerides and pleural drainage was continued. The patient was still receiving total parenteral nutrition (TPN) by POD 8 because of persistently high drainage output. As the drainage output gradually decreased, the patient was started on a low-fat diet once again. Left pleural effusion remained low and the thoracostomy tube was removed on POD 20. However, a chest X-ray showed a gradual increase in the left pleural effusion. On POD 29, left pleural drainage was repeated and we confirmed that the chylothorax had become exacerbated. We planned a surgical procedure to treat the intractable postoperative chylothorax because conservative treatment was unsuccessful.

We considered that a second surgery through the thoracic approach could be invasive for patients with postoperative complication after EPP. Furthermore, if surgery proceeded through the left thorax, complete repair of the leakage might not be feasible and further reconstruction of the chest wall might be required. Surgery through the right thorax without one-lung ventilation was also likely to be complicated. Therefore, we clipped the thoracic duct through a laparoscopic transhiatal approach on POD 37 to avoid surgery through the right or left thorax. To distend the thoracic duct and facilitate its identification, the patient was given ice cream 1 hour preoperatively. The patient was placed supine with the legs abducted under general anesthesia to place the 6 abdominal access ports. The hepatic left lobe was mobilized and the lesser omentum was divided to identify the crus of the diaphragm, which were dissected at the level of the aortic hiatus, and the esophagus was identified. The surrounding tissue was dissected along the esophagus and the aorta was extended along the mediastinum. The thoracic duct was identified at the right side of the aorta and clipped (Fig 1) and distension of thoracic duct on the near side of the clips was confirmed. This procedure was effective and the pleural effusion decreased. The thoracostomy tube was removed 7 days after the second surgery and the patient was discharged on POD 30.

Comment

Postoperative chylothorax is a rare complication with a reported incidence ranging from less than 1% to 2.4% of all thoracic surgery procedures [5, 6]. Furthermore, the reported incidence of postoperative chylothorax after EPP is 6% to 8% [1, 2], and it might be even higher. This

Accepted for publication Nov 28, 2011.

Address correspondence to Dr Tsubokawa, Department of Surgical Oncology, Research Institute for Radiation Biology and Medicine, Hiroshima University, 1-2-3 Kasumi, Minami-Ku, Hiroshima 734-8551, Japan; e-mail: international-1@hotmail.co.jp.

Published by Elsevier Inc

0003-4975/$36.00
doi:10.1016/j.athoracsur.2011.11.070

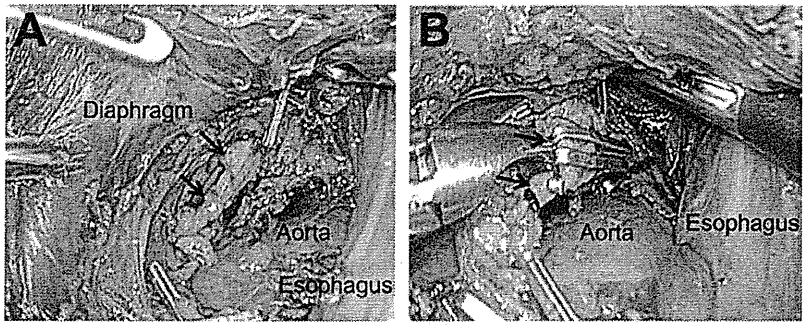

Fig 1. Thoracic duct clipped at right side of aorta. Arrows indicate thoracic duct (A) before and (B) after clipping.

is probably due to aggressive resection along the thoracic aorta and the mediastinum.

Various treatment modalities from conservative to operative intervention have been proposed. The initial management of chylothorax has traditionally been conservative and it includes drainage, TPN, a medium chain triglyceride diet, and octreotide. Surgical intervention is indicated when large amounts of chyle leakage persist after conservative treatment. Selle and colleagues [7] have recommended surgical intervention when the average daily chyle loss exceeds 1,500 mL, if chyle flow has not diminished for up to 14 days, or when nutritional complications appear imminent. Another report has indicated that if chyle leakage remains above 200 mL per day beyond 2 weeks after starting a conservative approach, then the treatment should be considered unsuccessful [8]. Our patients initially underwent drainage, a medium chain triglyceride diet, and TPN. This strategy temporarily diminished the large volume of chyle flow.

However, chyle leakage recurred after the chest tube was removed, so surgical treatment was considered. Ligation of the thoracic duct and repair of the leakage using sutures or clips through thoracotomy or video-assisted thoracic surgery (VATS) has become the standard approach to surgical intervention for chylothorax [1, 8]. Video-assisted thoracic surgery has recently become increasingly popular due to easy manageability and low morbidity [8]. However, the surgical procedures through thoracic approach were difficult for our patient. Surgery proceeding through the left thorax would have required a second reconstruction of the chest wall.

Furthermore, to find and completely repair the leakage at 1 month after a previous surgery was doubtful. Moreover, ligation of the thoracic duct through the right thorax was considered difficult because one-lung ventilation was impossible after left EPP. Surgery without one-lung ventilation would require open thoracotomy with a long incision that would be highly invasive and might cause adverse effects in the unaffected right lung after EPP. Therefore, clipping the thoracic duct through a laparoscopic approach was considered the most appropriate strategy for managing the persistent chylothorax in this patient.

Laparoscopic thoracic duct clipping is safe and minimally invasive even for patients with surgical complications, and particularly useful when a thoracic approach is unsuitable. We believe that this is a useful option for managing chylothorax.

References

1. Stewart DJ, Martin-Ucar AE, Edwards JG, West K, Waller DA. Extra-pleural pneumonectomy for malignant pleural mesothelioma: the risks of induction chemotherapy, right-sided procedures andprolonged operations. Eur J Cardiothorac Surg 2005;27:373–8.
2. Opitz I, Kestenholz P, Lardinois D, et al. Incidence and management of complications after neoadjuvant chemotherapy followed by extrapleural pneumonectomy for malignant pleural mesothelioma. Eur J Cardiothorac Surg 2006; 29:579–84.
3. Nair SK, Petko M, Hayward MP. Aetiology and management of chylothorax in adults. Eur J Cardiothorac Surg 2007;32: 362–9.
4. Krug LM, Pass HI, Rusch VW, et al. Multicenter phase II trial of neoadjuvant pemetrexed plus cisplatin followed by extrapleural pneumonectomy and radiation for malignant pleural mesothelioma. J Clin Oncol 2009;27:3007–13.
5. Cerfolio RJ, Allen MS, Deschamps C, Trastek VF, Pairolero PC. Postoperative chylothorax. J Thorac Cardiovasc Surg 1996;112:1361–6.
6. Shimizu K, Yoshida J, Nishimura M, Takamochi K, Nakahara R, Nagai K. Treatment strategy for chylothorax after pulmonary resection and lymph node dissection for lung cancer. J Thorac Cardiovasc Surg 2002;124:499–502.
7. Selle JG, Snyder WH III, Schreiber JT. Chylothorax: indications for surgery. Ann Surg 1973:177:245–9.
8. Fahimi H, Casselman FP, Mariani MA, van Boven WJ, Knaepen PJ, van Swieten HA. Current management of postoperative chylothorax. Ann Thorac Surg 2001;71:448–51.

Interactive CardioVascular and Thoracic Surgery 14 (2012) 5–11
doi:10.1093/icvts/ivr065 Advance Access publication 17 November 2011

INSTITUTIONAL REPORT

Radical hybrid video-assisted thoracic segmentectomy: long-term results of minimally invasive anatomical sublobar resection for treating lung cancer

Morihito Okada[a,*], Yasuhiro Tsutani[a], Takuhiro Ikeda[a], Keizo Misumi[a], Kotaro Matsumoto[a], Masahiro Yoshimura[b] and Yoshihiro Miyata[a]

[a] Department of Surgical Oncology, Research Institute for Radiation Biology and Medicine, Hiroshima University, Japan
[b] Department of Thoracic Surgery, Hyogo Cancer Center, Akashi, Hyogo, Japan

* Corresponding author. Tel: +81-82-2575869; fax: +81-82-2567109; e-mail: morihito@hiroshima-u.ac.jp (M. Okada).

Received 9 August 2011; received in revised form 28 September 2011; accepted 29 September 2011

Abstract

We analysed the results of radical segmentectomy achieved through a hybrid video-assisted thoracic surgery (VATS) approach that used both direct vision and television monitor visualization at a median follow-up of over 5 years. Between April 2004 and October 2010, 102 consecutive patients able to tolerate lobectomy to treat clinical T1N0M0 non-small cell lung cancer (NSCLC) underwent hybrid VATS segmentectomy in which we used electrocautery without a stapler to divide the intersegmental plane detected by selective jet ventilation in addition to the path of the intersegmental veins. Curative resection was achieved in all patients. The median surgical duration and blood loss during the surgery were 129 min (range, 60–275 min) and 50 ml (range, 10–350 ml), respectively. The complication rate was 9.8% (10/102) with the most frequent being prolonged air leak, and there was no case of in-hospital death or 30-day mortality post procedure. Five and seven patients developed locoregional and distant recurrences, respectively. The overall and disease-free 5-year survival rates were 89.8% and 84.7%, respectively. Radical hybrid VATS segmentectomy including atypical resection of (sub)segments is a useful option for clinical stage-I NSCLC. The exact identification of anatomical intersegmental plane followed by dissection using electrocautery is critical from oncological and functional perspectives.

Keywords: Segmentectomy • Lung cancer • Video-assisted thoracic surgery • Sublobar resection

THORACIC ONCOLOGIC

INTRODUCTION

Advances in radiographic devices such as high-resolution computed tomography (CT) and the widespread practice of low-dose helical CT for screening have resulted in an extraordinary increase in the early detection of ever smaller non-small cell lung cancers (NSCLCs), such as bronchioloalveolar carcinoma, that might possibly have more indolent biological behaviour. This trend has rapidly changed clinical practice in thoracic surgery, and thus concern has arisen over unified strategies that include whole lobectomy to treat small peripheral cancers. Removing a relatively large volume of healthy lung tissue could result in a poorer quality of postoperative life, a higher frequency of operative morbidity and a decreased likelihood of having a second or even a third NSCLC resected, for which such patients would survive long enough to become at risk. We have therefore actively performed radical segmentectomy with lymph node assessment not only for high-risk but also for good-risk patients with small clinical stage-I NSCLC [1–4]. The outcomes of the randomized study conducted by the Lung Cancer Study Group demonstrated that sublobar resections including wedge resections resulted in a higher rate of local recurrence compared with lobectomy in patients with clinical T1N0M0 NSCLC [5]. Thus, the incidence of non-anatomical stapled wedge resection has escalated and many recent residency programs in thoracic surgery do not cover segmentectomy as a mandatory procedure. However, we and other expert surgeons perceive segmentectomy as a crucial basic technique that should be mastered by all thoracic surgeons [6, 7].

We previously reported a novel segmentectomy in which the intersegmental plane was identified using selective jet ventilation under bronchofiberscopy [8]. Consequently, the segment to be removed can be inflated, whereas those to be preserved are maintained while deflated, which is contrary to the conventional procedure. However, this allows clear visualization of the anatomical intersegmental line between the segment to be resected and that to be preserved. The actual surgical margin in the inflated segment can be adequately grasped and a good surgical field can be obtained even through video-assisted thoracic surgery (VATS) without the need to physically suppress the other segments and lobes using an instrument. In addition, the anatomical intersegmental plane can be precisely dissected by electrocautery without any stapling. This allows the saved adjacent segments to remain completely expansive so that pulmonary function after surgery can be maximal.

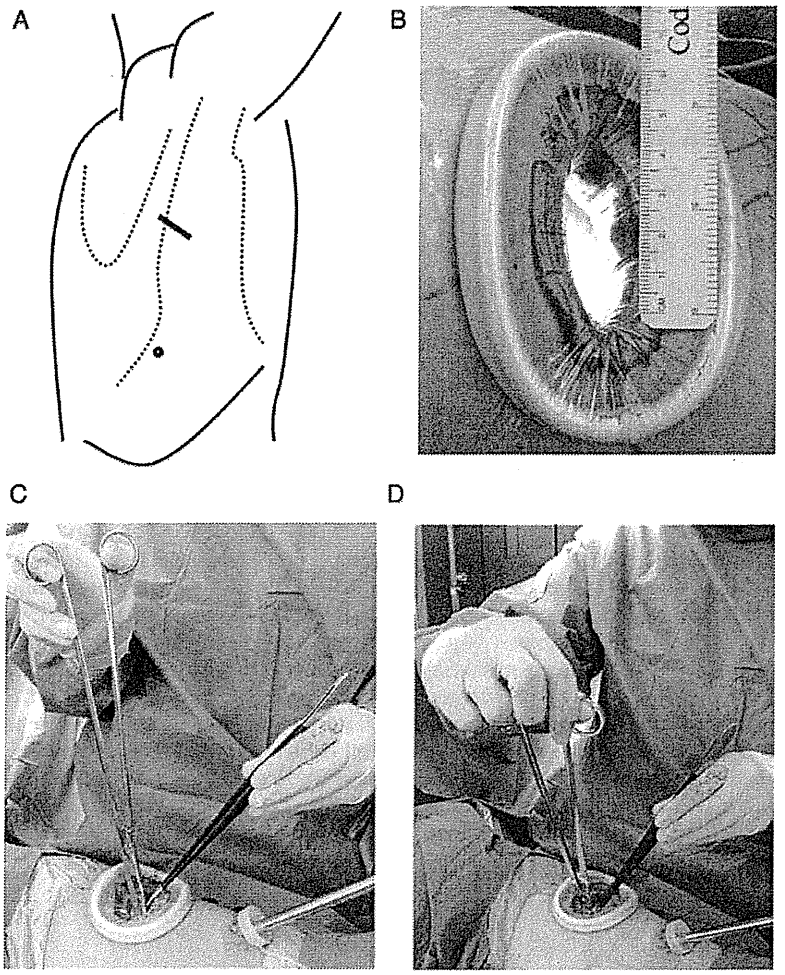

Figure 1: Hybrid VATS approach. (A) Skin is incised for one access port for a thoracoscope (circle) and for an access thoracotomy (solid line) over the mid-axillary line in the fourth interspace for upper or middle lobe tumours. Lower lobe tumours are approached through auscultatory triangle in the fifth interspace. (B) Operative exposure of about 4-cm wide is achieved using a wound retractor without rib spreading. (C and D) Sharp dissection in depths of an open thorax through direct vision is performed using an upside-down grip on 30-cm scissors, which allows manipulation with the thumb and index finger through the loops and flexible manoeuvring by turning up the wrist. The ulnar side of the hands rest comfortably alongside the margins of the incision, and awkward elevation of the forearms or elbows can be avoidable.

Basically, complete VATS using only a monitor for visualization is limited to lung resections of minimal difficulty and cannot be applied to all cancer surgeries, including segmentectomy and bronchoplasty. We have applied hybrid VATS, an integrated surgical approach that combines a muscle-sparing minithoracotomy and a thoracoscopic hole with television monitoring and direct visualization to expand the use of minimally invasive techniques for treating various malignant pathologies [9]. The present study analyses the surgical results of radical hybrid VATS segmentectomy at a median postoperative follow-up of over 5 years.

METHODS

Hybrid VATS segmentectomy

The hybrid VATS approach generally requires two skin incisions for access without cutting muscles or ribs [9]. One 4–5-cm incision is for manipulation and the other is an access port of 1-cm long for insertion of a thoracoscope (Fig. 1). The surgeon directly observes the hilum of the diseased lobe through the main access using a silicon rubber wound retractor with no rib spreading, and then individually isolates and severs all bronchi and vessels of the segment in question utilizing television monitor guidance when dissecting an area that is out of direct view. The skin incision was immediately extended when the surgeon has difficulty with the surgical view. Avoiding rib spreading is critical to the definition of a VATS approach. If the ribs were spread or a skin incision of ≥8 cm long was required, then the patient was excluded from the present study because it was considered a conversion to thoracotomy. We prefer a back hand grip to hold 30-cm-long scissors (model 101-8098-30; Mayo-Harrington; Stille, Sweden) for sharp dissection, long needle holders and forceps upside down (Fig. 1). Immediately after the insertion of a thoracoscope, subclinical dissemination of the tumour was checked by pleural lavage cytology [10].

The procedure of radical segmentectomy has been outlined in a previously published article [8]. Identifying the intersegmental plane with jet ventilation and cutting the intersegmental parenchyma using cautery are unique features of the procedure.

A 3.5-mm bronchofiberscope with a lighted tip that is visible at the surgical field is inserted into the orifice of the exposed targeted segmental bronchus. After selectively starting high-frequency oscillation (40 Hz, working pressure 2 kg/cm^2, HFO JET VENTILATOR, MERA, Tokyo, Japan), the diseased segments are inflated with air while the preserved segments appear collapsed, and a line is quickly and clearly formed between the inflated and the deflated parenchyma, demonstrating the anatomical intersegmental plane. This method is contrary to conventional inflation-deflation. The target bronchus is tied and cut with a suture or stapler to keep the segment inflated following being filled by jet ventilation. The surgeon can selectively introduce the tip of the fiberscope into each segmental/subsegmental bronchus and sequentially inflate segments/subsegments when more than one is scheduled for removal. At the proximal portion around the hilum, the intersegmental plane is approached along the intersegmental vein, and the plane is divided along the inflation-deflation line at the peripheral site using electrocautery. The margin must be greater than the diameter of the tumour and comprise at least 2 cm of unaffected lung tissue for controlling local recurrence. A few adjacent segments or subsegments should be removed unless the margin is sufficient. Air leakage at the bare surface of the preserved lung is controlled using an absorbable polyglycolic acid felt and a fibrin sealant consisting of fibrinogen and thrombin. Sampling or dissection of segmental, lobar, hilar and mediastinal lymph nodes followed by intraoperative frozen section analysis is mandatory to determine the applicability of segmentectomy. Standard lobectomy should proceed instead when the surgical margin is judged imperfect or any diseased lymph node is found. The chest is routinely drained using a single chest tube under water seal.

Although the simplest segments in order of easiest to hardest to remove are the upper division (S^{1-3}) and lingular segments (S^{4+5}) of the left upper lobe, the superior (S^6) and the basilar (right S^{7-10} or left S^{8-10}) segments of either lower lobe, we have aggressively performed complicated resection of segments/subsegments such as the left S^3 segment + S^{1+2}a subsegment (Fig. 2).

Patients

We performed radical hybrid VATS segmentectomy in which the intersegmental plane was divided using electrocautery without any stapling between April 2004 and October 2010 in 102 consecutive patients with clinical T1N0M0 NSCLC who could tolerate lobectomy. Surgical-pathologic staging was performed according to the New International Staging System for Lung Cancer [11]. Operative mortality was defined as death during hospitalization for pulmonary resection or within 30 days of the procedure, whichever was longer. Pathological cancer staging proceeded in accordance with the guidelines established by the American Joint Committee on Cancer [12]. Each patient provided his/her informed written consent based on the protocol approved by the institute's review board before surgery. After surgery, every patient was essentially evaluated every 3 months for the first 2 years and at 6-month intervals thereafter.

Statistical analysis

Overall and disease-free survival rates were estimated using the Kaplan-Meier method. Overall survival was defined as elapsed time from surgery until death from any cause or last follow-up. Disease-free survival was defined as elapsed time from surgery until the first diagnosis of local, regional or distant recurrent disease or until the last follow-up. We performed multivariate analyses using the Cox proportional hazards model to identify predictors of postoperative recurrence. Data were statistically analysed using SPSS software (version 10.5, SPSS Inc., Chicago, IL, USA).

RESULTS

Table 1 lists the characteristics of the 102 patients (52 women and 50 men; median age, 67 years; range, 34–89 years). Tumour size ranged from 8 to 29 mm (median; 18 mm). Most of the patients had an adenocarcinoma (91/102, 89.2%), of which a high proportion contained a bronchioloalveolar carcinoma component (58/91, 63.7%). Pathological assessments showed that curative resections were achieved with free surgical margins in all patients. Of all 102 patients with cT1N0M0 (stage-IA) disease, 84 (82.4%) were clinically staged as having T1a disease. Final pathological examination demonstrated that 92 (90.2%), 8 (7.8%), and 1 (1%) each had pathological stage IA, IB, IIA and IIIA disease, respectively. Table 2 shows the locations of the burdened segments. Actually, segmentectomy can be performed in any lobe except in the middle lobe, and no conversions to incisions longer than 8 cm were required in this series.

The operative results are shown in Table 3. The median operative time measured from skin incision to skin closure and median bleeding during surgery were 129 min (range, 60–274 min) and 50 ml (range, 10–350 ml), respectively. The median length of the skin incision for utility access was 50 mm (range, 40–80 mm). Postoperative complications developed in 10 patients (9.8%), with the most common being prolonged air leak in 4 patients (3.9%). Three patients (2.9%) had a late alveolopleural fistula requiring tube drainage, which is characteristic of our procedure as the intersegmental plane is divided without using a stapler. In 66 patients (64.7%), no air leak was observed at the time of surgery. The median postoperative duration of chest tube drainage was 1 day, that is, the drain was usually removed on the day following the procedure. None of the patients died while in hospital or during the 30 days after the procedure. Five deaths from cancer and four from other causes occurred during a median follow-up of 61 months (range, 8–84 months). Pleural dissemination/malignant effusion and mediastinal lymph node metastasis developed in two patients each and distant metastasis occurred in seven. Local margin recurrence that developed in one patient after lingulectomy was treated by completion left upper lobectomy, who has since remained recurrence free.

The overall and disease-free 5-year survivals of all patients were 89.8 and 84.7%, respectively (Fig. 3). Univariate analyses demonstrated that being male ($P = 0.0049$), having cancer other than adenocarcinoma ($P < 0.0001$) or a high CEA value ($P = 0.0070$) significantly and negatively affected disease-free survival (Fig. 4). Multivariate analysis showed that histological type ($P = 0.0133$) significantly correlated with risk for recurrence, whereas age ($P = 0.9880$), tumour size ($P = 0.4827$), skin incision ($P = 0.5623$), gender ($P = 0.0847$), side ($P = 0.9681$), lobe ($P = 0.4679$) and CEA value ($P = 0.6217$) did not (Table 4). Adenocarcinoma was therefore a significantly better independent prognostic determinant of recurrence.

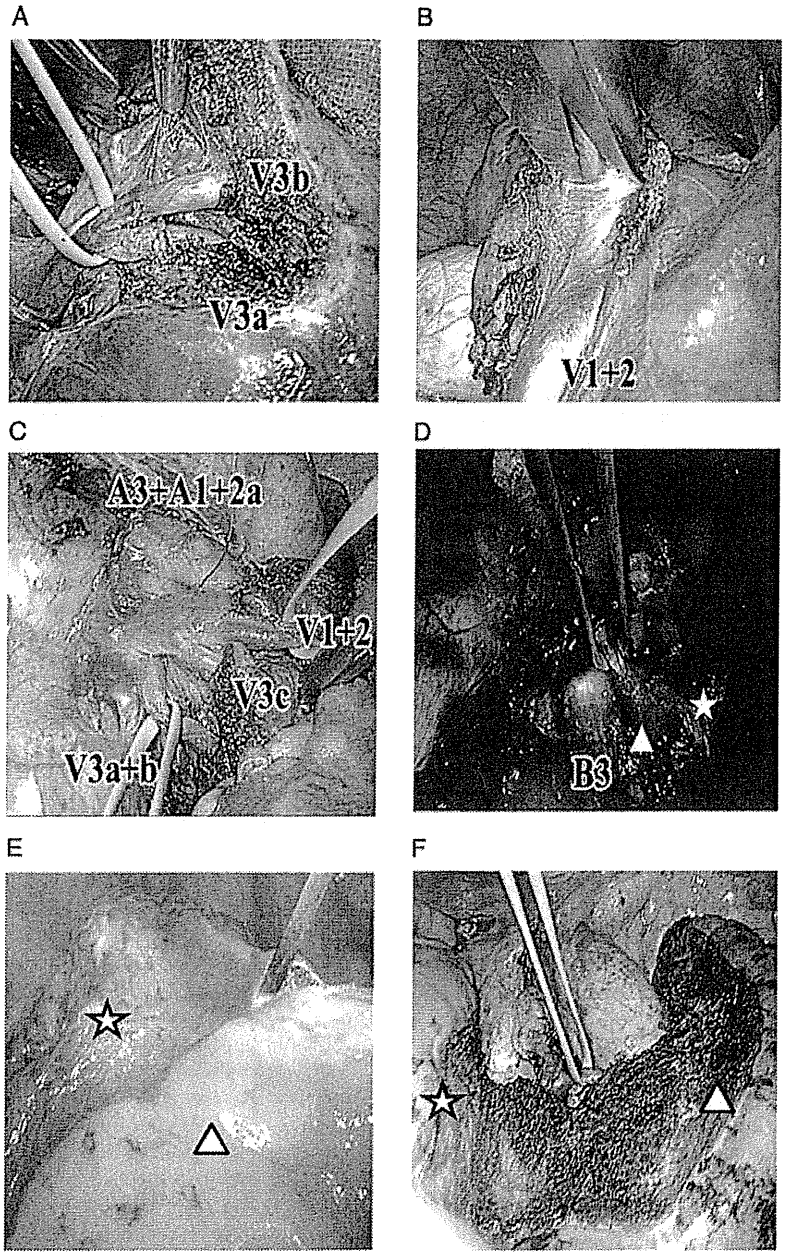

Figure 2: Left $S^3 + S^{1+2}a$ segmentectomy. (**A**) V^3a and V^3b branches of the vein running between upper division and lingular segment are identified and sufficiently exposed to distal portion. (**B**) Vein branch V^{1+2} is also exposed to distal site, and $V^{1+2}a$, $V^{1+2}b + c$ and V^{1+2} superior can be identified. $V^{1+2}a$ runs between S^3c and $S^{1+2}a$, and $V^{1+2}b + c$ runs between $S^{1+2}a$ and $S^{1+2}b + c$. (**C**) First two arterial branches (A^3 and $A^{1+2}a$) and vein branches ($V^{1+2}a$, $V^{1+2}b + c$, V^3a, V^3b and V^3c) are adequately exposed. Intersegmental branches of vein ($V^{1+2}b + c$, V^3b) are saved for venous return from preserved adjacent segments. (**D**) Bronchofiberscope through the double-lumen tube inserted into the orifice of the targeted segmental bronchus (B^3) in addition to $B^{1+2}a$ (star), where high-frequency oscillation is applied. $V^{1+2}b + c$ (triangle) is preserved. (**E**) Inflation–deflation line between and inflated (resected) $S^{1+2}a$ subsegment (triangle) and deflated (preserved) $S^{1+2}b + c$ subsegment (star) along which anatomical intersubsegmental plane is dissected with cautery. (**F**) Saved parenchyma of $S^{1+2}b + c$ (triangle) and S^4 (star) is fully inflated after removal of $S^3 + S^{1+2}a$.

DISCUSSION

The present study examined the relatively long-term outcomes of patients undergoing hybrid VATS segmentectomy, in which the intersegmental plane identified by the path of the intersegmental veins and by selective inflation of jet ventilation was divided by electrocautery without using a stapler. Because of the unavoidable selection bias in retrospective study, we could not compare the results between VATS segmentectomy and VATS lobectomy, which should be investigated in a prospective trial. The present study nevertheless showed that hybrid VATS segmentectomy is safe for treating patients with small clinical stage-I NSCLC and the results are excellent.

The approach via two skin incisions including a median minithoracotomy incision of 5 cm and a thoracoscope hole of 1 cm was minimally invasive, and none of our patients needed